Implications for familial hypercholesterolemia from the structure of the LDL receptor YWTD-EGF domain pair

Hyesung Jeon[1,2], Wuyi Meng[2,3], Junichi Takagi[4], Michael J. Eck[3], Timothy A. Springer[4] and Stephen C. Blacklow[1]

[1]Brigham and Women's Hospital and Harvard Medical School Department of Pathology, 75 Francis Street, Boston, Massachusetts 02115, USA. [2]These authors contributed equally to this work. [3]Dana Farber Cancer Institute and Harvard Medical School Department of Biological Chemistry and Molecular Pharmacology, 44 Binney Street, Boston, Massachusetts 02115, USA. [4]Center for Blood Research and Harvard Medical School Department of Pathology, 200 Longwood Avenue, Boston, Massachusetts 02115, USA.

The low-density lipoprotein receptor (LDLR) is the primary mechanism for uptake of cholesterol-carrying particles into cells. The region of the LDLR implicated in receptor recycling and lipoprotein release at low pH contains a pair of calcium-binding EGF-like modules, followed by a series of six YWTD repeats and a third EGF-like module. The crystal structure at 1.5 Å resolution of a receptor fragment spanning the YWTD repeats and its two flanking EGF modules reveals that the YWTD repeats form a six-bladed β-propeller that packs tightly against the C-terminal EGF module, whereas the EGF module that precedes the propeller is disordered in the crystal. Numerous point mutations of the LDLR that result in the genetic disease familial hypercholesterolemia (FH) alter side chains that form conserved packing and hydrogen bonding interactions in the interior and between propeller blades. A second subset of FH mutations are located at the interface between the propeller and the C-terminal EGF module, suggesting a structural requirement for maintaining the integrity of the interdomain interface.

The physiologic role of the low-density lipoprotein receptor (LDLR) is to carry cholesterol-containing lipoprotein particles into cells[1–3]. The primary ligand for the receptor is low-density lipoprotein, or LDL[1], which contains a single copy of apolipoprotein B-100; ~65–70% of plasma cholesterol in humans circulates in the form of LDL. Receptor–ligand complexes enter the cell by endocytosis at clathrin-coated pits, where receptor molecules cluster on the cell surface. Bound lipoprotein particles are subsequently released in the low pH milieu of the endosome, and the receptors then return to the cell surface in a process called receptor recycling[2].

The LDLR contains a series of discrete extracellular protein modules that are responsible for the binding and release of its lipoprotein ligands[4–6] (Fig. 1*a*). Adjacent to the seven N-terminal LDL-A modules, which are ~40-amino acid long tandem repeats that mediate binding to lipoproteins, is a 400-residue region of the receptor which encompasses two EGF-like modules, fol-

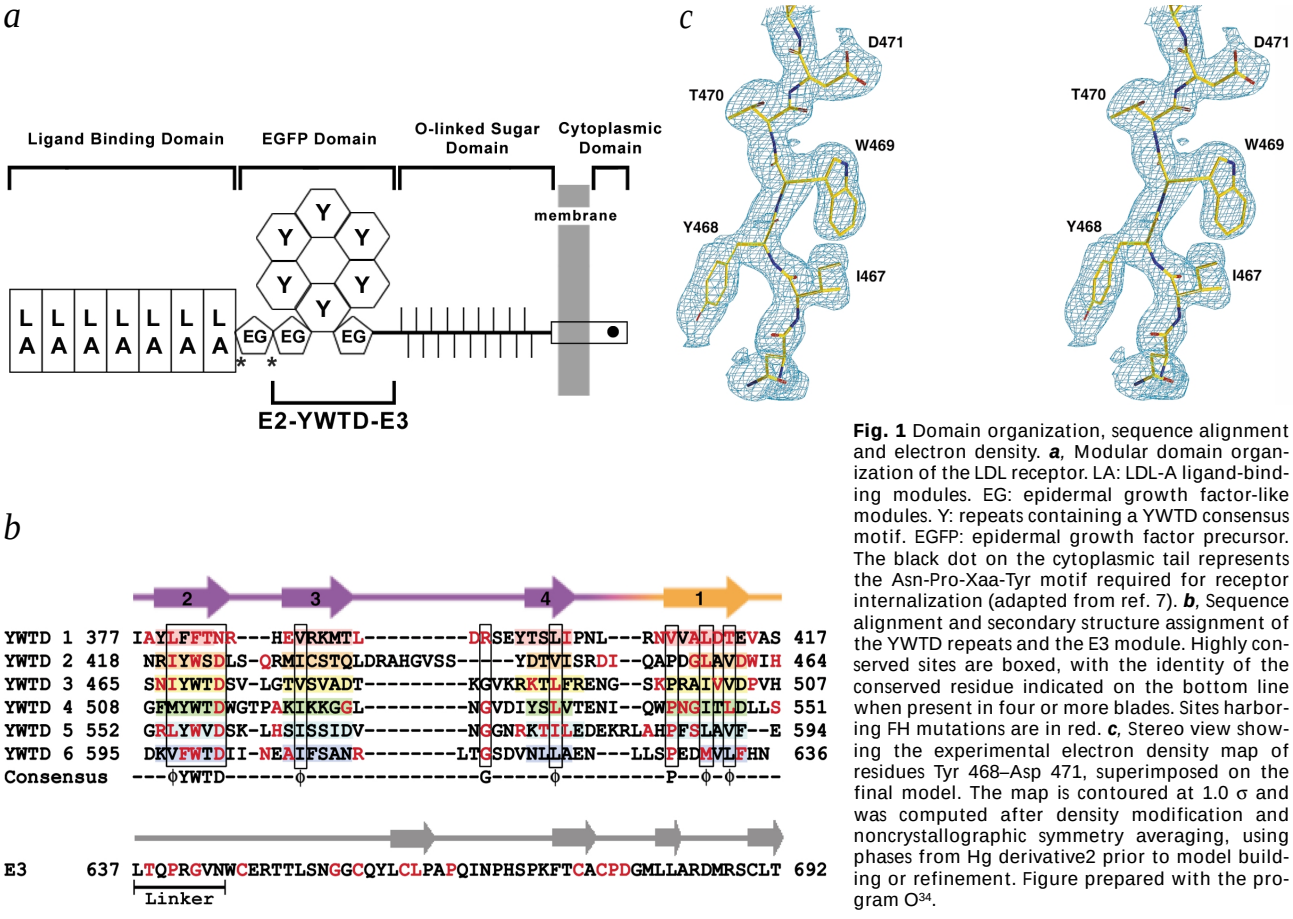

Fig. 1 Domain organization, sequence alignment and electron density. ***a***, Modular domain organization of the LDL receptor. LA: LDL-A ligand-binding modules. EG: epidermal growth factor-like modules. Y: repeats containing a YWTD consensus motif. EGFP: epidermal growth factor precursor. The black dot on the cytoplasmic tail represents the Asn-Pro-Xaa-Tyr motif required for receptor internalization (adapted from ref. 7). ***b***, Sequence alignment and secondary structure assignment of the YWTD repeats and the E3 module. Highly conserved sites are boxed, with the identity of the conserved residue indicated on the bottom line when present in four or more blades. Sites harboring FH mutations are in red. ***c***, Stereo view showing the experimental electron density map of residues Tyr 468–Asp 471, superimposed on the final model. The map is contoured at 1.0 σ and was computed after density modification and noncrystallographic symmetry averaging, using phases from Hg derivative2 prior to model building or refinement. Figure prepared with the program O[34].

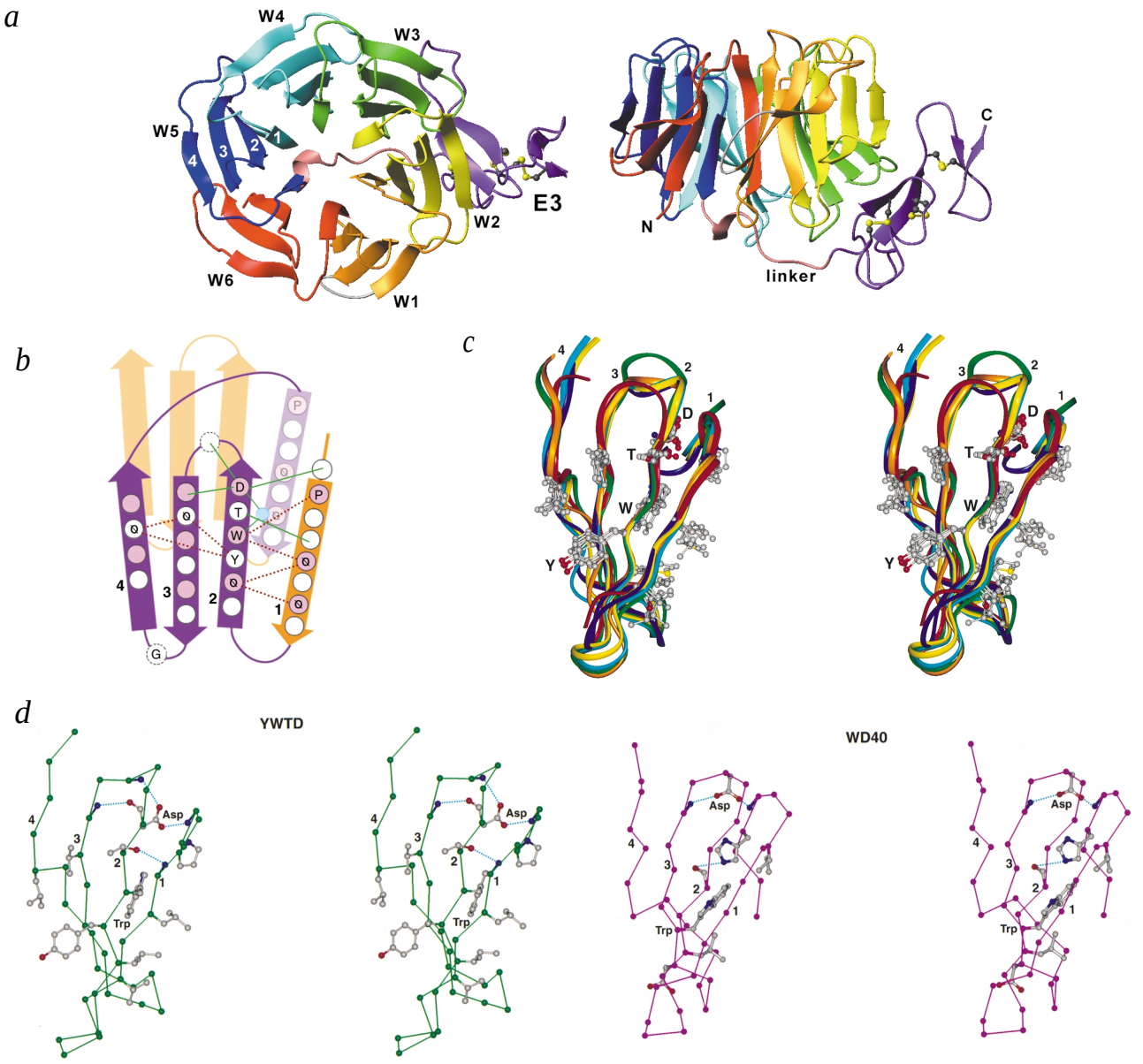

Fig. 2 Overview of structure and features of propeller blades. ***a***, Ribbon representation of the YWTD domain and adjacent C-terminal EGF-like module (E3) of the LDL receptor, colored to point out the six YWTD repeats of the six-bladed propeller. Left: view down the central axis of the six-bladed propeller; right: side view. Prepared using MOLMOL[38]. ***b***, Schematic representation of the interactions among consensus residues of each YWTD repeat, following the approach of Sondek *et al*[21]. Hydrogen bonds are illustrated with green lines and hydrophobic contacts with red dotted lines. White circles illustrate residues that face toward and pink circles face away from the viewer. The small blue circle represents the position of a water molecule. ***c***, Superposition of the six individual blades from the YWTD propeller. Stereo view in which side chains of conserved residues are illustrated on a ribbon trace of the backbone. ***d***, Stereo view comparison of the second YWTD blade from the LDLR (left) with a WD40 blade from the Gβ seven-bladed propeller[21] (right). Side chain and selected backbone hydrogen bonds from conserved Asp and Thr residues of the YWTD blade, and from conserved Asp and His residues of the WD40 blade, are illustrated by dashed light blue lines. Figure prepared using the program InsightII (MSI Inc.).

lowed by a series of six YWTD repeats[7] and a third EGF-like module (Fig. 1*b*). The part of the receptor harboring these EGF and YWTD repeats controls the related processes of lipoprotein release at low pH and recycling of the receptor to the cell surface[8].

The LDLR is a representative member of a subset of cell surface receptors that contain LDL-A, EGF (epidermal growth factor-like repeats) and YWTD (Tyr–Trp–Thr–Asp) modules arranged in a similar pattern (see refs 9,10 for reviews), and, more generally, serves as a prototype for all cell surface receptors containing YWTD repeats[7]. Receptors with YWTD domains control processes as diverse as lipoprotein uptake[2], clearance of protein complexes from plasma (for example see ref. 11) and the transmission of extracellular signals in development[12–18]. Other proteins with YWTD domains, often followed by an EGF-like module, include the *Drosophila* protein Arrow implicated in Wnt signaling[16], the extracellular matrix component nidogen and the tyrosine kinase sevenless (reviewed in ref. 7).

Protein expression and structure determination

The YWTD repeats have recently been predicted to fold into a YWTD domain — that is, a six-bladed β-propeller domain[7]. In order to understand the structure of this novel domain, its mode

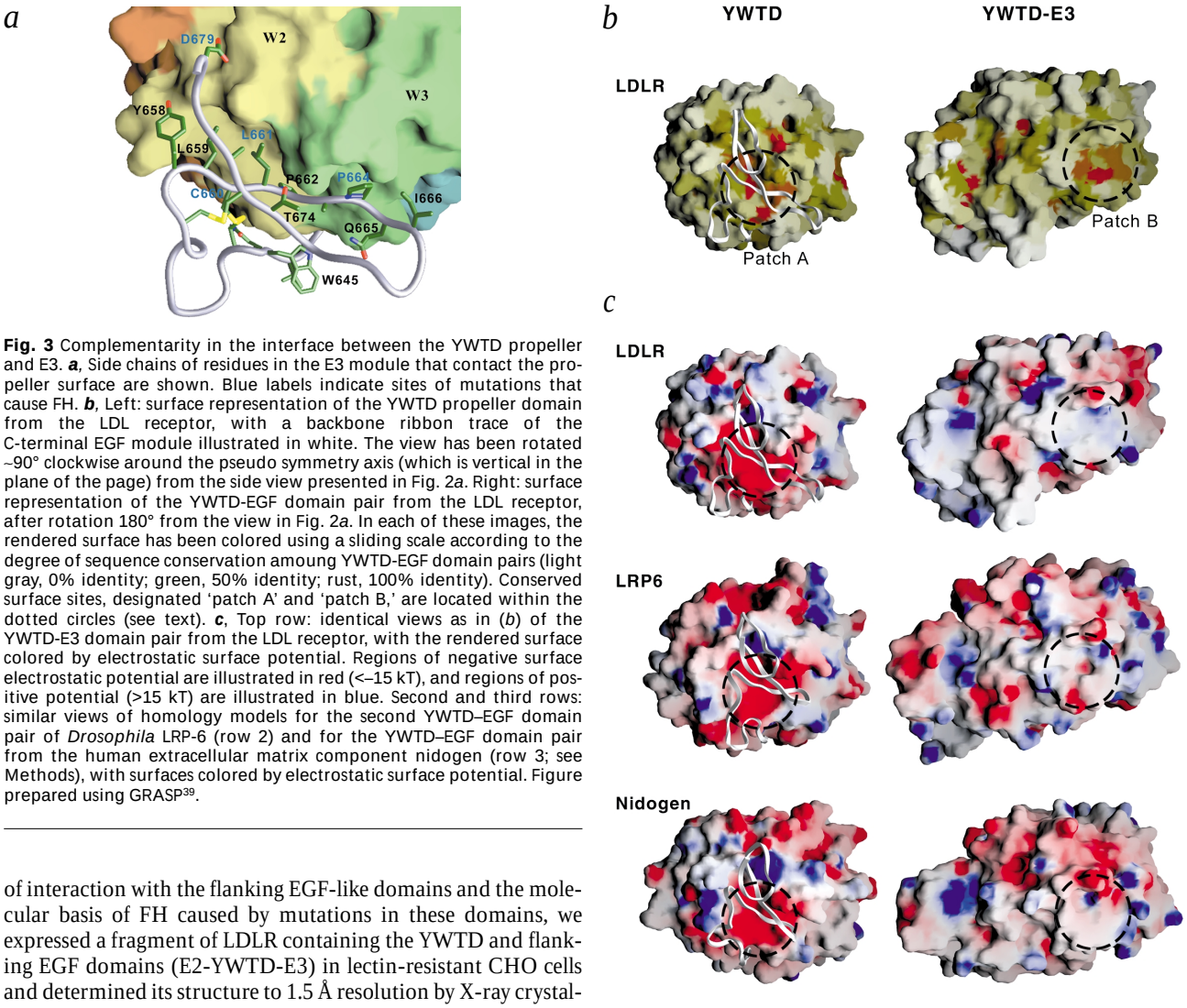

Fig. 3 Complementarity in the interface between the YWTD propeller and E3. ***a***, Side chains of residues in the E3 module that contact the propeller surface are shown. Blue labels indicate sites of mutations that cause FH. ***b***, Left: surface representation of the YWTD propeller domain from the LDL receptor, with a backbone ribbon trace of the C-terminal EGF module illustrated in white. The view has been rotated ~90° clockwise around the pseudo symmetry axis (which is vertical in the plane of the page) from the side view presented in Fig. 2*a*. Right: surface representation of the YWTD-EGF domain pair from the LDL receptor, after rotation 180° from the view in Fig. 2*a*. In each of these images, the rendered surface has been colored using a sliding scale according to the degree of sequence conservation amoung YWTD-EGF domain pairs (light gray, 0% identity; green, 50% identity; rust, 100% identity). Conserved surface sites, designated 'patch A' and 'patch B,' are located within the dotted circles (see text). ***c***, Top row: identical views as in (*b*) of the YWTD-E3 domain pair from the LDL receptor, with the rendered surface colored by electrostatic surface potential. Regions of negative surface electrostatic potential are illustrated in red (<–15 kT), and regions of positive potential (>15 kT) are illustrated in blue. Second and third rows: similar views of homology models for the second YWTD–EGF domain pair of *Drosophila* LRP-6 (row 2) and for the YWTD–EGF domain pair from the human extracellular matrix component nidogen (row 3; see Methods), with surfaces colored by electrostatic surface potential. Figure prepared using GRASP[39].

of interaction with the flanking EGF-like domains and the molecular basis of FH caused by mutations in these domains, we expressed a fragment of LDLR containing the YWTD and flanking EGF domains (E2-YWTD-E3) in lectin-resistant CHO cells and determined its structure to 1.5 Å resolution by X-ray crystallography (Fig. 1*c*). The structure includes two independent copies of the YWTD repeats and the adjacent C-terminal EGF-like module (E3) of the LDLR (Table 1) in the asymmetric unit of the crystal. The EGF-like module preceding the YWTD repeats (E2) appears to be disordered and is not visible in the electron density map.

Overview of structure

The six YWTD repeats together fold into a six-bladed β-propeller, consisting of six four-stranded β-sheets ('blades') arranged radially about a central pseudo symmetry axis (Fig. 2*a*). Along this axis is a central channel, 8–9 Å in diameter, filled with water molecules that form hydrogen bonds with backbone and side chain donors and acceptors from the β-strands lining the channel. The β-propeller model of the proposed[7] YWTD repeat domain of the LDLR is topologically accurate, with a root mean square (r.m.s.) deviation of 2.5 Å for all Cα atoms (1.09 Å for 124 core residues) compared to the crystal structure. To our knowledge, this degree of accuracy in the prediction of the three-dimensional structure of a ~250-residue, all β-protein domain that lacks sequence homology to any known structure is unprecedented in *de novo* structure prediction[19].

Each blade of the propeller consists of four antiparallel β-strands; the innermost strand of each blade is labeled 1 and the outermost strand, 4 (ref. 20). The sequence repeats are offset with respect to the blades of the propeller, such that any given 40-residue YWTD repeat spans strands 2–4 of one propeller blade and strand 1 of the subsequent blade (Figs 1*b*, 2*a*). This offset ensures circularization of the propeller because the last strand of the final sequence repeat acts as an innermost strand 1 of the blade that harbors strands 2–4 from the first sequence repeat. The linker following this last strand 1 connects the propeller to E3 by running along the base of the propeller.

Packing of conserved residues in individual blades

Except in blade 6 (W6), which varies from the others because of the discontinuity resulting from the circularization requirement, interactions among a set of conserved residues stabilize each individual blade and position adjacent blades of the propeller with respect to one another (Fig. 2*b*; ref. 21). The residues of the YWTD motif, which lies at the N-terminus of each imperfect 40-residue repeat, specify key positions of strand 2 within each blade (Fig. 2*b*,*c*). The conserved Asp residue of each YWTD motif serves several crucial roles in defining and stabilizing the propeller structure. The Asp terminating each strand 2 participates in backbone hydrogen bonds with the first residue of the

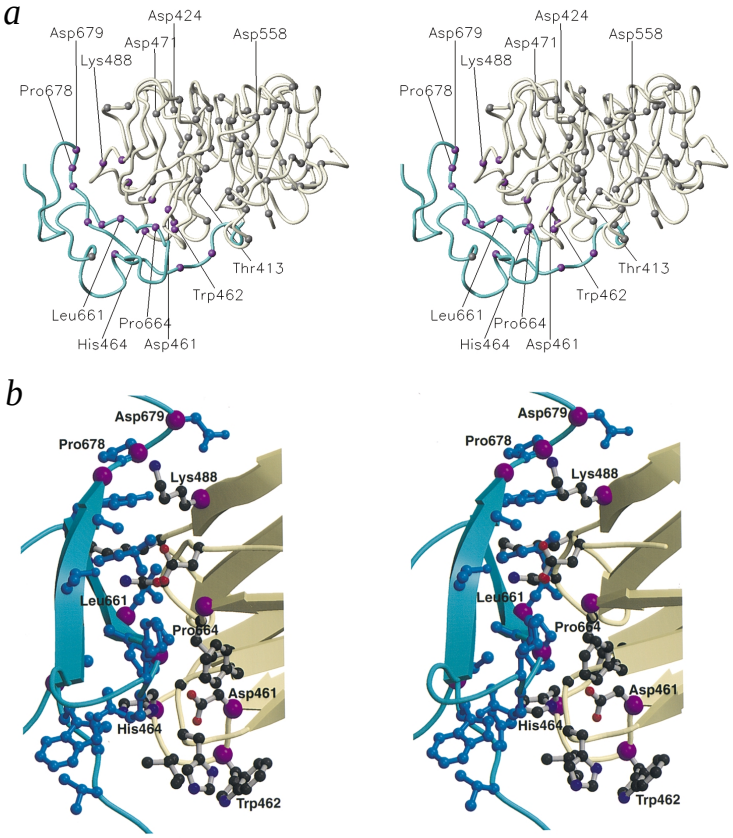

Fig. 4 Sites of FH mutations mapped onto the structure of the YWTD-EGF domain pair. ***a***, Stereo ribbon trace of the YWTD-E3 structure highlighting the Cα positions of all sites implicated in FH. The ribbon representing the YWTD domain backbone is khaki-colored, and the ribbon for the EGF module is turquoise. Cα atoms of FH sites outside of the interdomain interface are colored gray; Cα of interface sites harboring FH mutations are colored purple. Figure prepared with the program MOLMOL[38]. ***b***, Close-up of the YWTD-EGF interface region. Side chains of residues in the interface are shown in ball and stick representation, with residues from E3 in blue and residues from the YWTD propeller colored according to atom type. Cα atoms of interface sites harboring FH mutations are colored purple. Figure prepared with Molscript[40].

adjacent strand 3 (Fig. 2*b*). One of the carboxylate oxygen atoms of the aspartate side chain forms a hydrogen bond to a backbone amide in the connecting loop between strand 4 of the preceding blade and the adjacent strand 1 (4–1 loop), serving as a clasp between adjacent blades of the propeller. The other carboxylate oxygen of the aspartate usually participates in a water-mediated hydrogen bond with the indole nitrogen of the Trp residue preceding it within the YWTD motif (Fig. 2*b*). Conserved hydrophobic residues packed in the interior of the propeller establish the interfaces between adjacent blades.

As a result of these hydrogen bonding and side chain packing interactions among critical conserved residues within the 40-amino acid repeats, the six blades superimpose with r.m.s. deviations for backbone atoms of 0.8–1.2 Å, with better superposition of inner than of outer strands (Fig. 2*c*). Even though the YWTD sequence repeats have no obvious primary sequence similarity to WD40 (β-transducin) repeats of other propellers, the YWTD blades are close structural homologs of a typical WD40 blade from the seven-bladed propeller of the G-protein β-subunit (Gβ)[21–23] (Fig. 2*d*). Conserved Trp and Asp residues that are not in equivalent backbone positions in the two classes of propeller blades still carry out analogous structural roles. In each case, the Asp residue provides a side chain hydrogen bond to a backbone amide proton at the N-terminal end of strand 1 of its blade, and the Trp residue packs against hydrophobic residues from its blade and from the preceding blade to form a hydrophobic core. The high resolution structural information of several propellers with divergent primary sequence shows the variety of solutions to solving the topological problem of folding a propeller.

Interface between the YWTD and EGF modules

The interface between the YWTD domain and C-terminal EGF module observed in this structure provides a new model for interdomain relationships among modules of the LDLR family proteins[9,24] and explains why the YWTD propellers in all of these proteins are followed by an EGF-like module at their C-terminal end. The linker connecting the propeller to E3 packs tightly against the base of the propeller and contacts predominantly hydrophobic side chains in the 1–2 loops of blades two and three, situating E3 in contact with the second and third blades of the propeller (Fig. 3*a*). A total of ~1,400 Å^2 are buried in the interface between the propeller and E3, and an additional 900 Å^2 are buried in the contact surface between the linker and the propeller; the amount of buried surface area is typical of protein–protein interfaces[25]. Both molecules in the asymmetric unit of the crystal retain the same interface between domains, and a remarkable degree of surface complementarity exists between the propeller domain and E3. The large interface area between the YWTD domain and the C-terminal EGF module, and the evolutionary conservation of the contact region on the YWTD domain (patch 'A', Fig. 3*b*) suggest that other members of the LDLR family will share this quaternary, or 'supermodular,' organization. In further support of this model, some of the residues within this patch produce an area of negative electrostatic potential, predicted to be conserved in models of related propellers, including YWTD domains from LDLR-related protein-6 (LRP-6) and the extracellular matrix component nidogen (Fig. 3*c*). Most of the buried surface area, however, results from the packing of hydrophobic side chains of the EGF-like module — for example, Trp 645, Leu 659, Leu 661–Pro 664 and Ile 666 — into a groove on the propeller defined by the 1–2 and 3–4 loops of blades two and three, and the outer strand of blade two. Substantial interfaces with adjacent subunits, modules or subdomains exist in other β-propeller proteins, including Gβ[21–23], clathrin[26] and Tup-1 (ref. 27).

Implications for understanding FH mutations

Familial hypercholesterolemia (FH), which affects one in 500 people worldwide, results from any of a number of mutations in the gene encoding the LDLR[28–30] (a current list of known FH mutations is available at *http://www.ucl.ac.uk/fh/*). Of these mutations, 54% are located in the EGFP-homology region of the LDLR and 34% among the YWTD repeats (Fig. 1*b*). FH is characterized clinically by an elevated concentration of plasma LDL and cholesterol, and the relationship between FH and coronary heart disease remains the most cogent illustration of the causal relationship between elevated cholesterol levels and coronary atherosclerosis[28].

Table 1 Data collection, phasing and refinement statistics

	Native1	Native2	Hg derivative1	Hg derivative2
Resolution (Å)	1.85	1.5	1.85	3.0
Space group	$p3_221$	$p3_221$	$p3_221$	$p3_221$
Unit cell				
a = b	76.471	76.284	76.217	76.297
c	265.633	265.445	265.291	265.010
$\alpha = \beta$ (°)	90	90	90	90
γ (°)	120	120	120	120
Molecules[1]	2	2	2	2
R_{sym} (%)	4.9	6.9	7.2	9.0
Reflections (all / unique)	339,616 / 76,442	543,455 / 127,540	215,883 / 135,921	61,687 / 27,156
I / σ (all / last shell)	21.6 / 4.63	22.7 / 2.02	11.0 / 2.01	14.5 / 6.31
Completeness (all / last shell; %)	97.8 / 90.0	88.3 / 55.8	92.5 / 74.9	95.7 / 94.0
R_{iso} (%)				21.4
Phasing power (centric / acentric)				1.43 / 1.26
R_{cullis} (centric / acentric)				0.55 / 0.76
FOM				0.3662
Number of sites				8
Refinement				
Refinement range (Å)		20.0 – 1.5		
Nonhydrogen atoms		4,863		
Water molecules		1,193		
R_{cryst} / R_{free} (%)		20.8 / 25.0		
R.m.s. deviation bond lengths (Å) / angles (°)		0.007 / 1.6		

[1]Per asymmetric unit

A multitude of FH mutations within the YWTD region of the receptor alter crucial conserved scaffolding residues of the propeller (Fig. 4). Generally, mutations of this type cluster in the inner strands and rarely occur at residues lying on the outer strands of the propeller blades. Among FH mutations are changes that alter each one of the conserved Asp residues in the YWTD motifs that anchor the propeller blades. Because both carboxylate oxygens of this conserved Asp residue are acceptors of structurally conserved hydrogen bonds, even conservative substitutions (like the D424E, D471N and D558N mutations; Figs 1*b*, 4*a*), are likely to disrupt the structure of the propeller and prevent efficient transport of the receptor to the cell surface, leading to FH. Many mutations of other conserved positions within the propeller blades — for example, the Gly residues of the 3–4 loops, the Pro residues initiating the first strands of blades W4–W6 and the Trp residues of the YWTD motifs — may similarly interfere with proper folding of the propeller domain (Fig. 4*a*).

Additional FH mutations are found at the interface between the YWTD and E3 modules, including outer strand mutations of the YWTD domain (Fig. 4*b*). Mutations of this type include T413K at the end of strand 1 in blade one (a linker contact site); D461H, W462R, and H464R of the 1–2 loop of blade two and the K488E mutation of the external face of strand 4 of blade two (Figs 1*b*, 4). Similarly, the FH mutations L661P, P664L, P678L and D679E alter side chains of E3 that directly contact the propeller. These findings suggest a requirement for maintaining the integrity of the interface between the propeller and the EGF-like module, and raise the intriguing possibility that the integrity of this interface may be modulated by the decrease in pH that triggers ligand release in the endosome. This possibility is consistent with the change in surface electrostatic potential at the interface predicted to occur upon titration of the two nearby His 464 and His 507 by shifting from pH 7 to pH 5.

Relevance to other YWTD-containing proteins

Evidence implicating YWTD domains in protein–protein interactions has emerged from several studies. The YWTD propeller domain and adjacent EGF-like module of the extracellular matrix component nidogen bind laminin, another major component of basement membranes, with nanomolar affinity[31]. LRP-6 from frogs binds to the developmental signaling protein Wnt[18] and has been implicated, along with its homologs in mice and flies, as a coreceptor in Wnt signaling[16–18]. What surfaces of a propeller–EGF structure might be the binding interface of LDLR homologs, such as LRP-6 and nidogen? Binding *via* the bottom face of the propeller is unlikely, because the short linker that connects E2 to the N-terminal YWTD motif of the LDLR propeller would position E2 along the bottom face of the propeller near E3. Two other possibilities, however, are consistent with this topological constraint. First, a binding interface might incorporate the hydrophobic 'patch B' site (Fig. 3*b*,*c*, right panels), which includes residues from the outer strands of blades three and four and is conserved among YWTD propellers (Fig. 3*b*,*c*). Alternatively, protein–protein interactions between YWTD propellers and their binding partners may occur on the top face of the propeller, in a binding mode analogous to recognition of the heterotrimeric G-protein α-subunit by Gβ, as predicted[7], or use a composite interface defined by the propeller and its adjacent EGF-like domains.

Methods

Protein expression, purification and crystallization. E2-YWTD-E3 containing a C-terminal His_6-tag was produced in lectin-resistant CHO cells using the expression plasmid pEF1/V5-His (Invitrogen). Cleared cell medium was gently rocked in the presence of Ni-NTA

agarose beads (Qiagen) overnight, and recombinant protein was eluted from the beads with 250 mM imidazole, pH 8.0. The eluate was dialyzed against 50 mM Tris-HCl, pH 8.5; fractionated by anion-exchange chromatography on a Mono-Q column (Pharmacia) using a linear gradient of NaCl and purified to a single band on SDS-PAGE by gel-filtration (Superdex 200, Pharmacia) in 50 mM Tris-HCl buffer (pH 8.5) containing 0.3 M NaCl. All purification steps were carried out at 4 °C. Fractions containing E2-YWTD-E3 were pooled and concentrated to 10 mg ml^{-1} for crystallization.

Crystals were grown by vapor diffusion in hanging drops at room temperature by mixing one volume of concentrated protein solution (10 mg ml^{-1}) with one volume of a reservoir solution containing 0.1 M HEPES (pH 7.5), 10% (v/v) 2-propanol and 20% (w/v) polyethylene glycol (PEG) 4000. The crystals were transferred to a cryostabilization buffer, containing reservoir solution plus 20% (v/v) glycerol , and flash-frozen by rapid immersion into liquid nitrogen. Mass spectrometry of a dissolved crystal showed that the N-terminal EGF-like module (E2) is present in the crystals, even though E2 is not visible in the electron density map.

Data collection and structure determination. All diffraction data except those from 'Hg derivative2' were collected at –165 °C using the Quantum-4 CCD detector (ADSC) on the A1 beam line at CHESS (Cornell High Energy Synchrotron Source). Hg derivative2 data were collected using a rotating anode source (Rigaku RU-200EBH) with a MAR300 image-plate (Mar Research). Reflection data were indexed, integrated and scaled using the programs DENZO[32] and SCALEPACK[32].

Heavy atom sites were located by difference Patterson and difference Fourier methods using the program CNS[33]. The initial phases were calculated using the data from Hg derivative2 and were improved after combining them with Hg derivative1 data (Table 1). An electron density map was calculated using these phases with density modification and noncrystallographic symmetry averaging at 1.9 Å resolution. A model with two molecules in the asymmetric unit was then built manually using the graphics program O[34]. The initial model was refined using simulated annealing and the initial B-factor corrections with the combined native2 data to 1.5 Å using CNS. Final refinement of the 1.5 Å resolution model was completed with the program ARP/wARP[35].

Modeling and computer graphics. The 'lsq_e' and 'lsq_i' commands in O[34] were used to superimpose the six propeller blades and to calculate r.m.s deviations. Sequence alignments for 88 complete YWTD–E3 pairs, performed using the program PRPP[36], are from Springer[7]. The sequence entropy calculations used to prepare the surface representations in Fig. 3*b* were performed with a program written by S.E. Choe (unpublished results). Homology modeling of the LRP-6 and nidogen YWTD–E3 structures was performed using the program modeller4 (ref. 37). Electrostatic potential calculations for the YWTD domain were performed in the absence of the EGF module to prepare the left-hand panels of Fig. 3*c*.

Coordinates. The coordinates have been deposited in the Protein Data Bank (accession code1IJQ).

Acknowledgments
We thank J.-H. Wang for helpful discussions, F. Poy for assistance with computer graphics, S.E. Choe for the program *homology*, and C. Heaton and the staff at CHESS for assistance with synchotron data collection on beamline A1. This research is supported by NIH grants to S.C.B, T.A.S. and M.J.E. S.C.B. is a Pew Scholar in the Biomedical Sciences. This work is based upon research conducted at the Cornell High Energy Synchrotron Source (CHESS), which is supported by the National Science Foundation, using the Macromolecular Diffraction at CHESS (MacCHESS) facility, which is supported by the National Institutes of Health.

Correspondence should be addressed to S.C.B. *email: sblacklow@rics.bwh.harvard.edu*

Received 22 December, 2000; accepted 13 March, 2001.

1. Goldstein, J.L. & Brown, M.S. *J. Biol. Chem.* **249**, 5153–5162 (1974).
2. Brown, M.S. & Goldstein, J.L. *Science* **232**, 34–47 (1986).
3. Brown, M.S. & Goldstein, J.L. *Proc. Natl. Acad. Sci. USA* **71**, 788–792 (1974).
4. Yamamoto, T. *et al. Cell* **39**, 27–38 (1984).
5. Sudhof, T.C., Goldstein, J.L., Brown, M.S. & Russell, D.W. *Science* **228**, 815–822 (1985).
6. Sudhof, T.C., Russell, D.W., Goldstein, J.L. & Brown, M.S. *Science* **228**, 893–895 (1985).
7. Springer, T.A. *J. Mol. Biol.* **283**, 837–862 (1998).
8. Davis, C.G. *et al. Nature* **326**, 760–765 (1987).
9. Willnow, T.E., Nykjaer, A. & Herz, J. *Nature Cell Biol.* **1**, E157–162 (1999).
10. Herz, J., Gotthardt, M. & Willnow, T.E. *Curr. Opin. Lipidol.* **11**, 161–166 (2000).
11. Herz, J., Clouthier, D.E. & Hammer, R.E. *Cell* **71**, 411–421 (1992).
12. Hafen, E., Basler, K., Edstroem, J.-E. & Rubin, G.M. *Science* **236**, 55–63 (1987).
13. Simon, M.A., Bowtell, D.D.L. & Rubin, G.M. *Proc. Natl. Acad. Sci. USA* **86**, 8333–8337 (1989).
14. Hiesberger, T. *et al. Neuron* **24**, 481–489 (1999).
15. Trommsdorff, M. *et al. Cell* **97**, 689–701 (1999).
16. Wehrli, M. *et al. Nature* **407**, 527–530 (2000).
17. Pinson, K.I., Brennan, J., Monkley, S., Avery, B.J. & Skarnes, W.C. *Nature* **407**, 535–538 (2000).
18. Tamai, K. *et al. Nature* **407**, 530–535 (2000).
19. Moult, J. *Curr. Opin. Biotechnol.* **10**, 583–588 (1999).
20. Murzin, A.G. *Proteins Struct. Func. Genet.* **14**, 191–201 (1992).
21. Sondek, J., Bohm, A., Lambright, D.G., Hamm, H.E. & Sigler, P.B. *Nature* **379**, 369–374 (1996).
22. Wall, M.A. *et al. Cell* **83**, 1047–1058 (1995).
23. Lambright, D.G. *et al. Nature* **379**, 311–319 (1996).
24. Willnow, T.E. *J. Mol. Med.* **77**, 306–315 (1999).
25. Conte, L.L., Chothia, C. & Janin, J. *J. Mol. Biol.* **285**, 2177–2198 (1999).
26. ter Haar, E., Musacchio, A., Harrison, S.C. & Kirchhausen, T. *Cell* **95**, 563–573 (1998).
27. Sprague, E.R., Redd, M.J., Johnson, A.D. & Wolberger, C. *Embo J.* **19**, 3016–3027 (2000).
28. Goldstein, J.L., Hobbs, H.H. & Brown, M.S. In *The metabolic and molecular bases of inherited disease*, Vol. 2 (eds. Scriver, C.S., Beaudet, A.L., Sly, W.S. & Valle, D.) 1981–2030 (McGraw Hill Inc., New York; 1995).
29. Wilson, D.J. *et al. Am. J. Cardiol.* **81**, 1509–1511 (1998).
30. Varret, M. *et al. Nucleic Acids Res.* **26**, 248–252 (1998).
31. Fox, J.W. *et al. EMBO J.* **10**, 3137–3146 (1991).
32. Otwinowski, Z. & Minor, W. *Methods Enzymol.* **276**, 307–326 (1997).
33. Brunger, A.T. *et al. Acta Crystallogr. D* **54**, 905–921 (1998).
34. Jones, T.A., Zou, J.Y., Cowan, S.W. & Kjeldgaard, M. *Acta Crystallogr. A* **47**, 110–119 (1991).
35. Lamzin, V.S. & Wilson, K.S. *Acta Crystallogr. D* **49**, 129–147 (1993).
36. Gotoh, O. *J. Mol. Biol.* **264**, 823–838 (1996).
37. Sali, A. & Blundell, T.L. *J. Mol. Biol.* **234**, 779–815 (1993).
38. Koradi, R., Billeter, M. & Wuthrich, K. *J. Mol. Graph.* **14**, 51–55, 29–32 (1996).
39. Nicholls, A., Sharp, K.A. & Honig, B. *Proteins* **11**, 281–296 (1991).
40. Kraulis, P.J. *J. Appl. Crystallogr.* **24**, 946–950 (1991).